
**Liquid Crystals**
Publication details, including instructions for authors and subscription information:
http://www.informaworld.com/smpp/title~content=t713926090

# Temperature dependence of the properties of simulated PCH5

Sergei Ye. Yakovenko; Anatoli A. Muravski; Frank Eikelschulte; Alfons Geiger

Online publication date: 06 August 2010

**To cite this Article** Yakovenko, Sergei Ye. , Muravski, Anatoli A. , Eikelschulte, Frank and Geiger, Alfons(1998) 'Temperature dependence of the properties of simulated PCH5', Liquid Crystals, 24: 5, 657 — 671
**To link to this Article: DOI:** 10.1080/026782998206768
**URL:** http://dx.doi.org/10.1080/026782998206768

LIQUID CRYSTALS, 1998, VOL. 24, NO. 5, 657–671

# Temperature dependence of the properties of simulated PCH5

by SERGEI YE. YAKOVENKO, ANATOLI A. MURAVSKI
Institute of Applied Physics Problems, Minsk, Belarus

FRANK EIKELSCHULTE and ALFONS GEIGER*
Physical Chemistry, University of Dortmund, Germany

(*Received 30 April 1997; in final form 21 November 1997; accepted 5 December 1997*)

We present the results of molecular dynamics simulation studies of 4-(*trans*-4′-pentylcyclohexyl)-benzonitrile (PCH5) at different temperatures in the isotropic and nematic phases within the united atom approach. Special attention is paid to the electrostatic interactions. Different methods of determining point charges are compared and the effect of the electrostatic interactions on the molecular distribution is considered. Their decisive influence on local molecular packing and phase transition temperature is shown. We analyse various static and dynamic properties, being specially interested in the reliability of the simulation results, to check to which extent they are distorted by the confinements adopted during the simulations (and especially the size of the system). Using realistic molecular interaction models in contrast to simple model ellipsoids, we find that the number of molecules and the lengths of the simulation runs have to be increased considerably when studying macroscopic properties like the phase transition temperature and the order parameter. Much easier to access are single particle and local properties such as translational dynamics and local ordering, but also the relative dependence of the order parameters of various ranks.



## 1. Introduction

Since the first computer simulation studies of nematic liquid crystals [1] molecular dynamics (MD) became a conventional method of research in this field. Using simplified molecular models, like hard ellipsoids [2], rigid Lennard-Jones rods [3, 4] or particles interacting via the Gay–Berne potential [5], explanations for many specific features of the mesophase were found. The success of these simulations encouraged MD studies of systems with more realistic interaction potentials (based on detailed atom–atom interactions) to get closer contact to real liquid crystalline compounds and to be in a position to reproduce the properties of real substances (essentially this is determined by the quality of the force field). Certainly, such modifications of the potential lead to a considerable increase in computation time. Nevertheless, within this approach successful simulations of nematic liquid crystals [6–9] and even more complex states like chiral nematic [10] and smectic C* (a single freely suspended layer with ferroelectric structure) [11] phases have been performed. An explicit treatment of molecular flexibility and electrostatic interactions enabled a detailed investigation of local molecular ordering in the nematic and isotropic phases of mesogens and comparison with experimental results.

*Author for correspondence.

Simulations of simplified molecular models have given evidence for a variety of mesophases in such systems [12]. It was shown there that having 256 molecules in the system it is possible to trace through the phase transition by a series of simulation runs of several hundred picoseconds each. This intriguing perspective of performing detailed computer studies of such intricate phenomena as transitions to the mesophase of realistic liquid crystal materials has led us to extend our previous simulations of PCH5 at $T = 330$ K [13] to a larger temperature range.

This paper is organized as follows. In § 2 we analyse the interaction potential (especially its electrostatic part) and the simulation procedure. In § 3 we consider the equilibration process and the temperature dependence of various properties. Brief conclusions from this discussion are presented in § 4.

## 2. Computational methods and interaction model

In this paper we present the results of molecular dynamics simulation studies of the nematic and isotropic phase of 4-(*trans*-4′-pentylcyclohexyl)benzonitrile (PCH5). For the simulations the GROMOS package [14] was used. In this package the aliphatic $CH_2$ and $CH_3$ and the aromatic CH groups are treated in the united atom approximation (UA), i.e the hydrogens are included in the parameters of the carbon atoms so that a single

molecule consists of 19 interaction sites (see figure 1). The total potential energy as a function of the internal degrees of freedom and interatomic distances is represented in a symbolic manner by:

$$U = \frac{1}{2}\sum_{\theta} K_\theta(\theta - \theta_0)^2 + \frac{1}{2}\sum_{\xi} K_\xi(\xi - \xi_0)^2 + \sum_{\phi} K_\phi[1 + \cos(n\phi - \delta)] + \sum_{i<j}\left(\frac{A_{ij}}{r_{ij}^{12}} - \frac{B_{ij}}{r_{ij}^{6}} + \frac{1}{4\pi\varepsilon_0}\frac{q_i q_j}{r_{ij}}\right) \quad (1)$$

where $K_\theta$, $K_\xi$, $K_\phi$ are force constants representing bond bending, out-of-plane bending and torsional potentials, respectively. The distance between interacting sites $i$ and $j$ is $r_{ij}$. $A_{ij}$ and $B_{ij}$ are the parameters of the Lennard–Jones potential and $q_i$ is the partial charge on site $i$. The force field parameters are taken from GROMOS and given in tables 1–6.

The SHAKE algorithm [15] is used to fix bond lengths and to eliminate the high frequency bond stretching motion, so that it is possible to integrate the equations of motion with a timestep of 2 fs. The simulated systems contain 200 molecules using a rectangular box by employing periodic boundary conditions. In all runs the box was anisotropic, approximately $l_x \simeq 2{\cdot}9$ nm; $l_y \simeq 4{\cdot}8$ nm; $l_z \simeq 7{\cdot}0$ nm.

The interactions were calculated with the minimum image convention using a cut-off radius of 1·2 nm. The simulations were performed at constant pressure $p = 1$ atm and constant temperature using the Berendsen

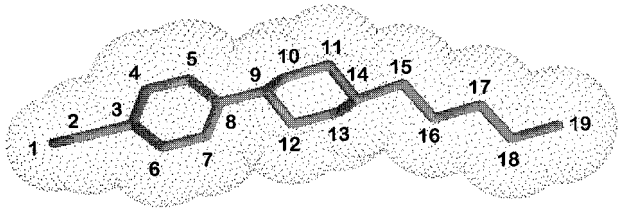


Figure 1. United atom model and atom-numbers of PCH5.

Table 1. GROMOS atom-types and corresponding atom-numbers from figure 1.

| Type | Number |
|---|---|
| N | 1 |
| C | 2 |
| CB | 3, 8 |
| CA | 4, 5, 6, 7 |
| CS1 | 9, 14 |
| CS2 | 10, 11, 12, 13, |
| $CH_2$ | 15, 16, 17, 18 |
| $CH_3$ | 19 |

Table 2. Bond lengths for SHAKE.

| Bond | $b_0$/Å |
|---|---|
| N–C | 1·33 |
| C–CB | 1·53 |
| CB–CA | 1·39 |
| CA–CA | 1·39 |
| CB–CS1 | 1·53 |
| CS1–CS2 | 1·53 |
| CS2–CS2 | 1·53 |
| CS1–$CH_2$ | 1·53 |
| $CH_2$–$CH_2$ | 1·53 |
| $CH_2$–$CH_3$ | 1·53 |

Table 3. Bond bending parameters.

| Angle | $K_\theta$/kJ mol$^{-1}$ rad$^{-2}$ | $\theta_0$/° |
|---|---|---|
| N–C–CB | 577·68 | 180·0 |
| C–CB–CA | 481·40 | 120·0 |
| CB–CA–CA | 481·40 | 120·0 |
| CB–CS1–CS2 | 288·84 | 109·5 |
| CS1–CS2–CS2 | 288·84 | 109·5 |
| CS1–$CH_2$–$CH_2$ | 529·54 | 111·0 |
| $CH_2$–$CH_2$–$CH_2$ | 529·54 | 111·0 |
| $CH_2$–$CH_2$–$CH_3$ | 529·54 | 111·0 |

Table 4. Parameters for torsional potentials.

| Torsional angle | $K_\phi$/kJ mol$^{-1}$ | $n$ | $\delta$ |
|---|---|---|---|
| $X$–CB–CS1–$Y$ | 0·4814 | 6 | 0 |
| $X$–CS1–CS2–$Y$ | 6·7369 | 3 | 0 |
| $X$–CS2–CS2–$Y$ | 6·7369 | 3 | 0 |
| $X$–CS1–CS2–$Y$ | 6·7369 | 3 | 0 |
| $X$–$CH_2$–$CH_2$–$Y$ | 6·7369 | 3 | 0 |

Table 5. Parameters for out of plane bending.

| Torsional angle | $K_\xi$/kJ mol$^{-1}$ rad$^{-2}$ | $\xi_0$/° |
|---|---|---|
| $X$–CA–CA–$Y$ | 192·56 | 0·0 |
| $X$–CA–CB–$Y$ | 192·56 | 0·0 |
| $X$–C–CA–$Y$ | 192·56 | 0·0 |

algorithm [16]. The time constant of pressure relaxation (by varying the box dimensions) was chosen to be $\tau_p = 5{\cdot}0$ ps to avoid unrealistic collective oscillations in the mesophase. For $\tau_T$ we chose 0·01 ps.

Because of the importance of electrostatic interactions for the behaviour of liquid crystals, we carefully determined the partial charges of PCH5. The partial charges were chosen such that they represent the electrostatic potential obtained by *ab initio* quantum mechanical calculations performed with GAUSSIAN 92 [17] (potential derived charges). For this purpose, we first performed a Hartree–Fock geometry optimization using

Table 6. Parameter for non-bonded interactions. Parameters marked by (1–4) refer to intramolecular interactions across three bonds. The other values refer to further intramolecular separations and all intermolecular interactions. Mixed interaction parameters $A_{ij}$ and $B_{ij}$ are calculated from the given values according to the mixing rules used in GROMOS [14].

| Atom-type | $A_{ii}/(10^6\,\mathrm{kJ\,mol^{-1}\,\AA^{12}})$ | $B_{ii}/(10^3\,\mathrm{kJ\,mol^{-1}\,\AA^{6}})$ |
|---|---|---|
| N | 1·954 | 2·802 |
| C | 3·880 | 2·691 |
| CB | 3·880 | 2·691 |
| CA | 17·398 | 6·345 |
| CA(1–4) | 9·585 | 6·359 |
| CS1 | 82·554 | 14·379 |
| CS1(1–4) | 4·299 | 3·351 |
| CS2 | 40·654 | 10·466 |
| CS2(1–4) | 8·184 | 5·430 |
| $CH_2$ | 40·654 | 10·466 |
| $CH_2$(1–4) | 8·1838 | 5·430 |
| $CH_3$ | 30·088 | 10·215 |
| $CH_3$(1–4) | 13·879 | 7·885 |

the 6-31G* basis set and then fitted the Coulomb potential of the charges placed at the atomic sites to the electrostatic potential obtained from the *ab initio* calculations. Both the full-atom (FA) and the UA approach were used during fitting. These procedures led to substantially different sets of charges, even for atoms not connected with hydrogens. Even though the full atom charge fit resulted in a better representation of the *ab initio* electrostatic potential, we used the UA set of charges, because the UA model is adopted in GROMOS. These charges are presented in table 7.

To eliminate artefacts due to the appearance of non-compensated charges when applying the interaction cut-off, the charges in the molecule were slightly adjusted to form three neutral charge groups (the benzonitrile fragment, the cyclohexane ring and the pentyl chain). The cut-off for electrostatic interaction was taken with respect to the centre of mass distance between such groups.

Simulations were performed at the temperatures given in table 8. Equilibration periods varied between 100 s and 500 ps, depending on the starting configuration.

### 2.1. *Notes on equilibration*

#### 2.1.1. *Translational diffusion*

To be sure that the properties which we discuss later do not depend on the initial conditions, we checked by several methods the relaxation of various properties of the system using the simulation of the isotropic phase. It is clear that translational order in a dense system cannot be equilibrated as long as the mean-square



Table 7. Partial charges for PCH5, CB5 and CCH5. Columns 3 and 5: Mulliken charges; column 4: atomic charges for PCH5 used in the simulation; column 6: charges used in [9]; column 7: charges used in ref. [18]. Note that in columns 3, 5 and 7 the charges of the hydrogens are added to the charges of the heavy atoms.

| | | Charges $q/e$ | | | | |
|---|---|---|---|---|---|---|
| | | PCH5 | | CB5 | | CCH5 |
| Atom-number | Atom-type | Mulliken | Fitted | Mulliken | Ref. [19] | Ref. [18] |
| 1 | N | −0·46 | −0·65 | −0·45 | −0·51 | −0·206 |
| 2 | C | 0·27 | 0·58 | 0·10 | 0·33 | 0·063 |
| 3 | CB | −0·02 | −0·10 | 0·30 | −0·07 | 0·046 |
| 4 | CA | 0·07 | 0·10 | −0·08 | 0·09 | 0·029 |
| 5 | CA | −0·01 | −0·10 | −0·07 | 0·03 | 0·006 |
| 6 | CA | 0·07 | 0·10 | −0·08 | 0·09 | 0·029 |
| 7 | CA | −0·03 | −0·10 | −0·07 | 0·03 | 0·006 |
| 8 | CB | 0·08 | 0·17 | 0·25 | −0·04 | 0·016 |
| 9 | CS1 | −0·04 | 0·20 | 0·25 | −0·07 | 0·013 |
| 10 | CS2 | 0·02 | −0·10 | −0·07 | 0·03 | −0·005 |
| 11 | CS2 | 0·01 | −0·10 | −0·06 | 0·02 | −0·003 |
| 12 | CS2 | 0·02 | −0·10 | −0·07 | 0·03 | −0·005 |
| 13 | CS2 | 0·01 | −0·10 | −0·06 | 0·02 | −0·003 |
| 14 | CS1 | −0·01 | 0·20 | 0·10 | −0·04 | 0·015 |
| 15 | $CH_2$ | 0·01 | 0·00 | 0·00 | 0·01 | −0·003 |
| 16 | $CH_2$ | 0·00 | 0·00 | 0·00 | 0·04 | −0·001 |
| 17 | $CH_2$ | 0·00 | 0·00 | 0·00 | 0·00 | 0·002 |
| 18 | $CH_2$ | 0·00 | 0·00 | 0·00 | 0·01 | 0·007 |
| 19 | $CH_3$ | 0·00 | 0·00 | 0·00 | −0·02 | −0·009 |
| Dipole moment/Debye | | 6·04 | 5·01 | 8·06 | 5·94 | 2·82 |

Table 8. Temperatures and lengths of simulation runs.

| Phase | Temperature/K | Production period/ps |
|---|---|---|
| Nematic | 300 | 500 |
| | 310 | 968 |
| | 320 | 1000 |
| | 330 | 800 |
| | 340 | 600 |
| | 350 | 674 |
| | 370 | 500 |
| | 400 | 900 |
| | 430 | 850 |
| | 450 | 600 |
| Isotropic | 310 | 400 |
| | 330 | 900 |
| | 350 | 400 |

displacement of the particles $\overline{\Delta r^2} = 6Dt$ is not of the order of their size. So we calculated the van Hove self correlation function $W(r)$, which is the probability density of a molecule to diffuse within time $t$ to a distance $r = |\mathbf{r}(0) - \mathbf{r}(t)|$. The results for the isotropic state at 330 K are presented in figure 2.

It is seen that an interval of 200 ps is long enough for molecules to diffuse through distances equal to the transversal molecular diameter. In 1 ns molecules will diffuse on average a distance equal to half of the molecular length. So for equilibration in the longitudinal direction probably not all of our simulation runs are sufficient. It should be noted that after about 500 ps the calculated van Hove probability for our system is very well described as a small-step diffusion process [20]:

$$W(r) = \frac{N(|\mathbf{r}(0) - \mathbf{r}(t)|)}{N_0} = 4\pi r^2 (4\pi D t)^{-3/2} \exp\left(-\frac{r^2}{4Dt}\right). \quad (2)$$

In fact, using the diffusion constant $D$ in equation (2) equal to the experimental value $1{\cdot}0 \times 10^{-10}\ \mathrm{m^2\,s^{-1}}$, obtained from NMR measurements [19] of PCH5 at 333 K, we get perfect coincidence with the curves obtained from the simulation.

### 2.1.2. *Rotational diffusion*

Probably even more important for nematics is orientational molecular motion, which is responsible for establishing orientational equilibrium. Some orientational autocorrelation functions

$$C_{Lm}(t) = \frac{\langle D^L_{m0}(0)\, D^{Is}_{m0}(t)\rangle}{\langle |D^L_{m0}(0)|^2\rangle} \quad (3)$$

(where $D^L_{m0}(t)$ are Wigner functions, characterizing orientation of the molecular fixed coordinate system [21], for which we took the benzonitrile fragment, in the laboratory frame at time $t$) are presented in figure 3 for the isotropic phase. Concerning tumbling motion (CF with $m = 0$) one can conclude from this figure that molecular reorientation (and hence reliable orientational equilibration) requires at least nanoseconds. The relaxation of the collective orientational order is an even

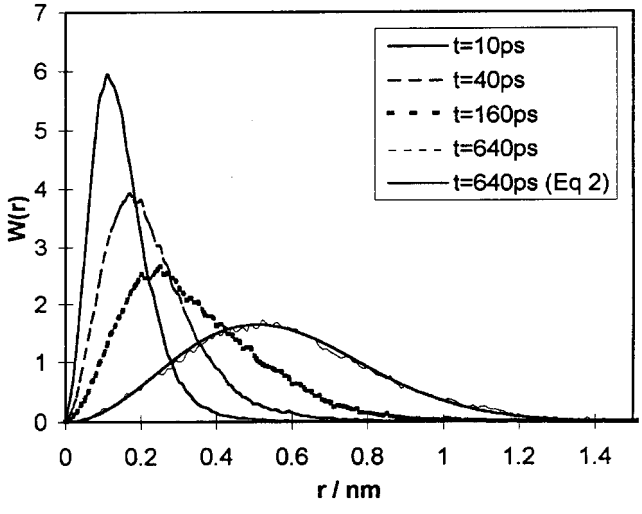


Figure 2. The probability of a molecule diffusing in time $t$ to a distance $r = |\mathbf{r}(0) - \mathbf{r}(t)|$ (van Hove self correlation function) for the isotropic state at 330 K, determined for various times. The solid line is computed with equation (2) and the experimental diffusion coefficient [19].

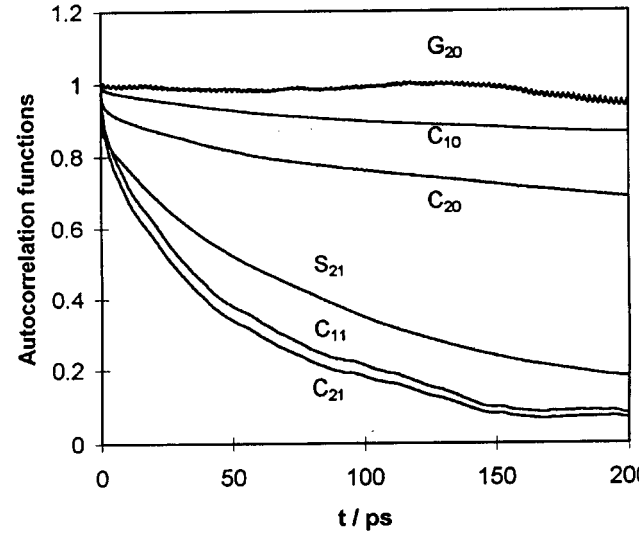


Figure 3. Orientational autocorrelation functions of various ranks for a molecular fixed frame—$C_{Lm}(t)$ of equation (3), a collective reorientation CF variable—$G_{Lm}(t)$ of equation (4), and the intramolecular orientational correlation functions $S_{21}(t)$ describing the reorientation of the bond 15–16 in the frame of the benzonitrile fragment. (Isotropic state at 330 K.)

much slower process. Figure 3 shows the many particle correlation function

$$G_{Lm}(t) = \frac{\sum_{j \neq i} \langle D^{L}_{m0}[\Omega_i(0)] D^{L*}_{m0}[\Omega_j(t)] \rangle}{\sum_{j \neq i} \langle D^{L}_{m0}[\Omega_i(0)] D^{L*}_{m0}[\Omega_j(0)] \rangle}. \qquad (4)$$

It is not possible to estimate from figure 3 how long it will take to establish equilibrium of the collective orientational variables of our simulated system. The well known relation of Keyes and Kivelson [22] relates a collective reorientation time $\tau_c$ with a single particle reorientation time $\tau_s$ by the orientational correlation parameter $g_2$, which we calculated to be about 8 for our system at 330 K [13]: $\tau_c = g_2 \times \tau_s$. From this one can conclude that, in contrast to the Lebwohl–Lasher lattice model [23], realistic molecular models of liquid crystals require orders of magnitude longer time for orientational equilibration, which is necessary for studying macroscopic orientational properties. Among the reasons for this one can mention the presence of electrostatic interactions and a much more complicated shape with conformational relaxation of the realistic molecules.

Despite this very slow tumbling, the spinning motion of mesogens is rather fast. Autocorrelation functions $C_{11}(t)$ and $C_{21}(t)$ relax in picoseconds (figure 3). The simulation time is also sufficient for intramolecular twisting conformational relaxation. From figure 3 it is seen that $S_{21}(t)$, which corresponds to twisting of the 15–16 bond around the molecular long axis, has a relaxation time less than 100 ps. The formula for $S_{21}(t)$ is similar to equation (3) with $D$-functions calculated for this bond in the molecular frame. So our simulations can be useful to study even intramolecular conformational statistics. Some more arguments concerning sufficiency of equilibration of local ordering of our system are also presented in the next part.



## 3. Properties

### 3.1. *Reference system*

Calculating the order parameters one can distinguish at least three reference systems. One is that of the simulation box. As can be seen [8], the box orientation has almost no connection with the director orientation although it may influence the value of the order parameter. It is appropriate to treat all orientation dependent properties relative to the nematic director orientation. We define such a frame as the one where the average tensorial order parameter of a molecular long axis, computed from the orientational vector $\mathbf{I} = (\mathbf{r}_{14} - \mathbf{r}_2)/|\mathbf{r}_{14} - \mathbf{r}_2|$, connecting atoms no. 2 and 14,

$$Q\alpha_\beta = \langle (3I\alpha I_\beta - \delta\alpha_\beta)/2 \rangle \qquad \alpha, \beta = x, y, z \qquad (5)$$

is diagonal. Averaging in equation (5) is performed over all molecules in the simulation box at a given time step. Certainly the director orientation is time dependent and one more coordinate system can be introduced, which is based on the *time average* of equation (5) over the whole simulation run. As has been shown in [24], nematic ordering is not orientationally stable for infinite three-dimensional systems in zero field and hence in our system with periodic boundaries, migration of the instant coordinate system defined by equation (5) should produce a uniform orientational distribution and the averaged orientation over the whole run loses its physical meaning. So unless specially mentioned, all the properties are presented in the instant coordinate system defined by (5).

### 3.2. *Order parameter* $P_2$

Single particle orientational properties of the mesophase are represented in general by single particle distribution functions and are conveniently described by orientational order parameters, the coefficients of their expansion in a series of Legendre polynomials. We are not interested in the macroscopic manifestation of the conformational flexibility, so we did not use the molecular inertia tensor to define the molecular orientation, but have chosen the line connecting two opposite carbon atoms in the phenyl and cyclohexane rings as the molecular long axis (atoms no. 2 and 14). Thus averages over the simulation run of the order parameters

$$P_1 = \langle \cos \Theta \rangle \quad \text{and} \quad P_2 = \langle (3 \cos^2 \Theta - 1)/2 \rangle \qquad (6)$$

for different temperatures are presented in figure 4. $\Theta$ is the angle between this axis and the eigenvector of $Q$ corresponding to the maximum eigenvalue. At first glance it is seen that the clearing point of the simulated system cannot be reproduced. In reality PCH5 becomes isotropic at 328 K, while the simulated system seems to be definitely melted only at 430 K. This stabilization of the orientational order originates not only from inappropriate interaction parameters, but from the insufficient equilibration and averaging. As is seen from figure 5, simulations at temperatures 300 to 350 K were started with an initial order parameter about $P_2 = 0{\cdot}7$ and at temperatures 370 to 450 K from $P_2 = 0{\cdot}65$. From the time evolution of the orientational ordering, it is seen that due to long-term fluctuations we cannot distinguish the order parameters in the range 300 to 400 K [in figure 4 (*a*) the error bars reflect the scattering of the instant values, presented in figure 5]. Only at higher temperatures do fluctuations of the order parameter noticeably increase [figure 4 (*a*), the lower curve]. If we start from a configuration with very low orientational order (isotropic system), then even at 330 K no tendency to increase the order is observed.

This metastability of the simulated system is confirmed by studies of the order parameter $P_1$. Sometimes the

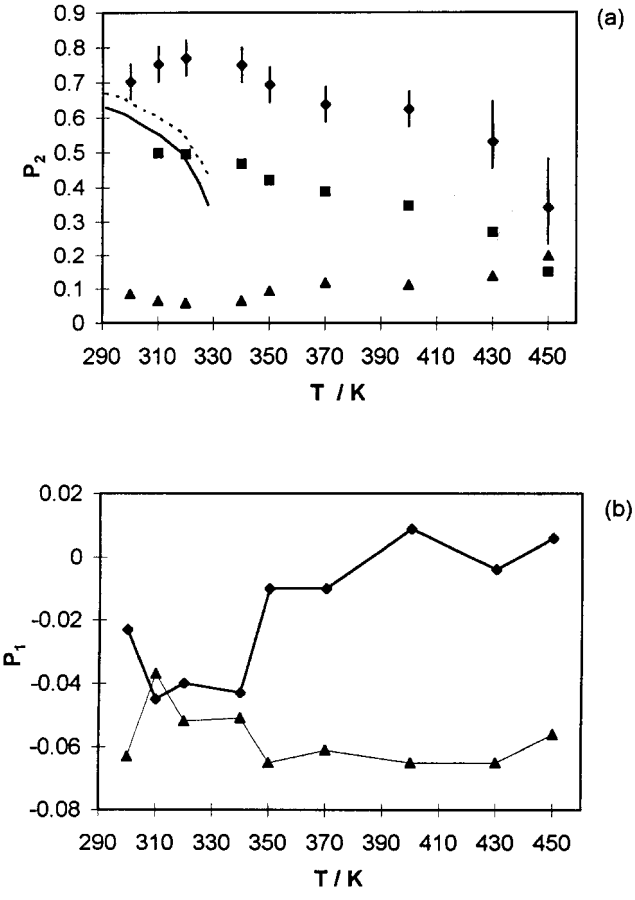


Figure 4. The temperature dependence of the order parameters $P_2$ (*a*) and $P_1$ (*b*) for the simulated system (diamonds). Squares are the finite-size corrected values. The mean square fluctuations $\delta P_2$ calculated with formula (7) are shown as triangles in (*a*). The square root of $P_1^{ij}$, calculated with equation (8), are given by triangles in (*b*). Curves show the experimental values for an infinite system (solid) and values it would have in a system with the size of the simulation box (dashed curve).

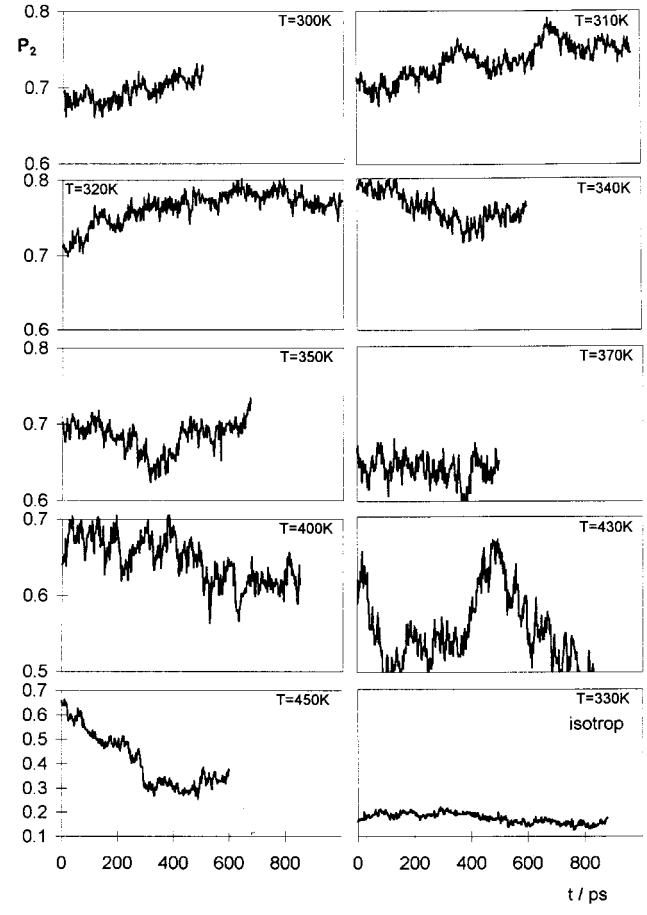


Figure 5. The time dependence of the order parameter $P_2$ for various temperatures. In all cases the scale is similar except for the two frames at the bottom.

simulated system can possess noticeable permanent polarization, which, in spite of its smallness, does not relax during the simulation run [figure 4 (*b*)]. In an additional check we interchanged the temperature of two runs (at 340 and 350 K), but no change of the order parameters beyond the fluctuation range was observed during 400 ps. Such striking differences of our systems from the behaviour of ellipsoids (see, for example [25], where some even more intricate phases were successfully simulated) makes us conclude that contemporary computer power is insufficient to reproduce unambigously such macroscopic properties as the phase transition temperature and the order parameter, simulating mesogens with realistic molecular interaction potential. It should be mentioned that the studies of another mesogen, 5OCB, have led the authors of [26] to similar conclusions. The question about the origin of this metastability arises. In the following sections we present various properties which were estimated for our system with the aim of checking to what extent they are distorted by the boundary conditions adopted during the simulations.

### 3.3. *Fluctuations of order parameters*

Fluctuations of the order parameters being also very important for the characterization of the mesophase, are probably more local properties than the order parameters themselves. Nevertheless, as is seen from figure 4 (*a*), fluctuations of $P_2$

$$\delta P_2 \equiv \langle (P_2 - \langle P_2 \rangle)^2 \rangle = 18\langle P_4 \rangle/35 + 2\langle P_2 \rangle/7 - \langle P_2 \rangle^2 + 1/5 \qquad (7)$$

are strongly coupled to $P_2$ itself. This simply reflects the course of $P_2$ and not an intrinsic temperature variation. It is especially well seen from the plot of $P_4$ [which is simply another parameter characterizing fluctuations of $P_2$, as can be seen from equation (7)] vs $P_2$. From

figure 6 it is seen that independent of temperature variations, $P_4$ follows very closely predictions of the fluctuation theory of Faber [27] (solid straight line).

Such properties as order parameters can also be calculated irrespective of any coordinate system:

$$P_1^{ij} = \langle \cos \Theta_{ij} \rangle \quad \text{and} \quad P_2^{ij} = \langle (3 \cos^2 \Theta_{ij} - 1)/2 \rangle \tag{8}$$

where $\Theta_{ij}$ denotes the angle between the long axes of a pair of molecules. It can be shown [28] that in the absence of orientational correlations between molecules $i$ and $j$, the defined parameters $P_1^{ij}$ are reduced to the conventional ones:

$$P_1^{ij} = (P_1)^2 \quad \text{and} \quad P_2^{ij} = (P_2)^2. \tag{9}$$

It is seen from figure 4 (*b*)—in which triangles represent the square root of $P_1^{ij}$ to compare it with $P_1$ from equation (6)—that $P_1$ calculated in this manner is not so much dependent on temperature as on non-relaxed ordering in the system. On the contrary, for $P_2$ we could not find significant differences between these values for our nematic systems. Only for the isotropic state did the square root of $P_2^{ij}$ occur about 10% higher than $P_2$. It should be noted that the presence of local order should be considered from the point of view of the difference between the order close to the central molecule and in the average in the system. In our case this means that in real systems the orientational correlation length is bigger than the box size and only in the isotropic phase are we able to observe the local ordering reliably.



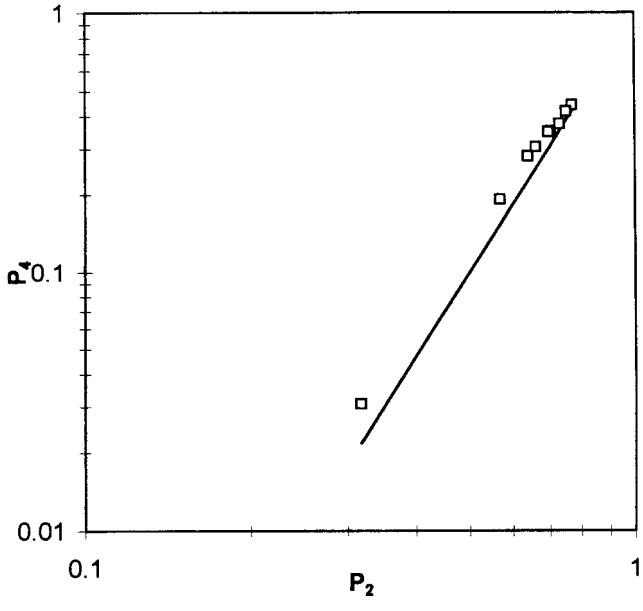


Figure 6. $P_4$ vs $P_2$ dependence for the simulated system (points) and according to the predictions of the continuum model [27] (solid line).

### 3.4. *Finite size corrections of order parameters*

One difference between the simulated system and the real substance is the application of periodic boundary conditions, introducing substantial differences between the degree of ordering in the simulation box and in an infinite system. The presence of periodic boundaries induces some orientational ordering even in the isotropic phase (see figure 5), moving the phase transition to higher temperatures and making it less sharp. To estimate how much the order parameters in the periodic box differ from those of an infinite system constituted of the same molecules, one can consider the simulation box to be the elementary volume of the nematic continuum. A set of modes is thermally excited which periodically distort the initially uniform director field of identical boxes placed in a periodic lattice (periodic boundary conditions). We then can use the formalism of continuum theory [24] to estimate the effect of the distortion modes with wavelengths from infinity down to the box dimensions which are missing in the simulation. The effect of shorter wavelength modes is already included in the orientational disorder of the molecules inside the box. Therefore we denote $P_L^{\text{loc}}$ the order parameters of the molecules in the box (Legendre polynomials of rank $L$). In the Appendix we derive expressions, showing how they are related to $P_L^{\text{lab}}$, the order parameters of the infinite fluctuating system, which we consider to be representative of the real substance:

$$P_L^{\text{lab}} = P_L^{\text{loc}} \exp\left\{ -\frac{1}{4} L(L+1) \sum_{\alpha} \frac{k_B T}{2\pi K_{\alpha\alpha} a_z} \times \left[ \varepsilon \arctan\left(\frac{1}{\varepsilon}\right) + \frac{1}{2} \ln(\varepsilon^2 + 1) \right] \right\} \tag{10}$$

$$\varepsilon = \frac{a_z}{a_\perp} \left( \frac{K_{\alpha\alpha}}{K_3} \right)^{1/2}$$

with $a_z$ and $a_\perp$ being the box dimensions parallel and perpendicular to the director. Using experimental values of the elastic constants $K_{\alpha\alpha}$ [29] we rescale the experimental order parameters [30] of real PCH5 to the size of our system. It is seen from figure 4 (*a*), that while the transition temperature as indicated by the temperature dependence of $P_2$ is raised, it could not be expected to rise to the value obtained in the simulations.

### 3.5. *Pair correlation functions*

Distribution functions of a different kind can be used to characterize the structure of liquid crystals. In the previous paragraphs we have considered orientational order parameters, which are in fact the coefficients of the expansion of the single particle orientational distribution function in a series of Legendre polynomials. They deliver information only on the averaged molecular

orientation in the bulk. The local molecular arrangement is given by $g(\mathbf{r}, \Omega)$—the pair distribution function. In liquid crystals $g(\mathbf{r}, \Omega)$ is a function of at least seven variables (two characterizing the relative position, and five the orientation relative to the director in the medium) and it is not an easy task to choose its proper representation.

Figure 7 shows the centre of mass radial distribution functions for the nematic and isotropic states at 330 K. Features beyond the first peak conventionally are attributed to the second environmental shell, but not in this case. For such a highly anisometric system, the radial distribution function is determined by a superposition of first and second neighbour shell contributions from different directions. For example, the broad peak between 1·0 and 1·5 nm in the isotropic phase is a superposition of the second shell perpendicular and the first shell parallel to the main axis of the reference molecule. (This can be seen from figure 11, which will be discussed below.)

In order to get a better understanding of the local molecular arrangement, we consider a two-dimensional distribution function. We therefore average over the molecular orientation of the neighbouring molecules. We neglect molecular flexibility and consider the centre of mass distribution $g_{12}(\mathbf{r}_{12})$, where $\mathbf{r}_{12}$ is the position-vector of molecule 2 in the frame of molecule 1 with the $z$ axis directed along the reference molecule 1 (the vector connecting atoms 3 and 14 was taken as the $z$ axis in these computations).

Neglecting the vanishing molecular biaxiality of the nematic phase, the number of variables is reduced to two: $z$ and $r^2 = (x^2 + y^2)$. The pair distribution function for nematic PCH5 at 330 K is shown in figure 8 (*a*). In this figure the reference molecule is pointing with its cyano group to the negative $z$ axis. Several maxima are clearly seen in it. Their coordinates $(z, r)$ in nm are:

$$(-1{\cdot}5, 0{\cdot}2), (-0{\cdot}7, 0{\cdot}5), (-0{\cdot}5, 0{\cdot}5) \quad \text{and} \quad (0{\cdot}5, 0{\cdot}5).$$

There is one more peak with $r = 1{\cdot}0$ nm which is extended from $z = -1{\cdot}0$ to 0·5 nm, parallel to the $z$ axis. These features of the distribution function reflect the specifics of molecular arrangement and molecular interactions. For a molecule with a plane of symmetry perpendicular to its long axis, the distribution function must also be symmetric relative to this plane. Real molecules lack this symmetry element, because of different substitutions (CN fragment on one side and flexible alkyl chain with carbon atoms 15–19 on the other; besides this, the molecule has an asymmetric charge distribution shown in table 7, which also breaks the symmetry of interactions).

To separate the factors that influence the asymmetry of the molecular arrangements, we did a computer experiment. In a system with well equilibrated local structure (200 molecules after 1 ns of equilibration) we switched off the electrostatic interactions. The dynamics of this system were observed over a period of 200 ps and some results are shown in figure 8. After 20 ps the peak at $(z, r) = (-1{\cdot}5, 0{\cdot}2)$ [figure 8 (*b*)] became smaller and after 100 ps [figure 8 (*c*)] it disappeared completely. Other features remained unchanged, so one can conclude that the peak that is lost originates from electrostatic interactions. (As will be seen later in the discussion of figure 12, this peak is formed essentially by antiparallel neighbours.) This change in the pair distribution function also changed other properties of the system considerably: the diffusion coefficient increased to $D_{\parallel} = 3{\cdot}5 \times 10^{-10}\ \mathrm{m^2\,s^{-1}}$ and $D_{\perp} = 2{\cdot}0 \times 10^{-10}\ \mathrm{m^2\,s^{-1}}$. The dynamics of the order parameter of this system after switch-off are displayed in figure 9. This continuously decreases to the isotropic value, and one can conclude that electrostatic interactions were decisive for the stability of the nematic order in this system.

To investigate further the dependence of the local structure on the molecular parameters we calculated the two-dimensional pair distribution function for other systems in various states. For a 100 molecule system [8] with charges positioned only at the cyano fragment, a comparable dependence of the peak height and position on the values of partial charges is observed (figure 10).

The isotropic phase was prepared from the nematic phase by heating the system to 540 K (the nematic phase isotropized at this temperature after 50 ps). After keeping it at this temperature for 300 ps the system was cooled to 330 K and equilibrated during 300 ps. The subsequent simulation run of 900 ps was then analysed. The long high temperature treatment of the system ensured the dissipation of all metastable arrangements remaining from the mesophase. After cooling, molecular interactions

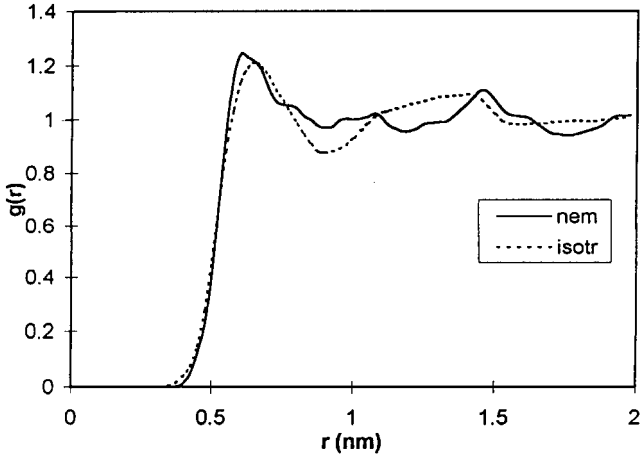


Figure 7. Centre of mass radial distribution functions for the system of 200 PCH5 molecules at 330 K in the nematic and isotropic states.

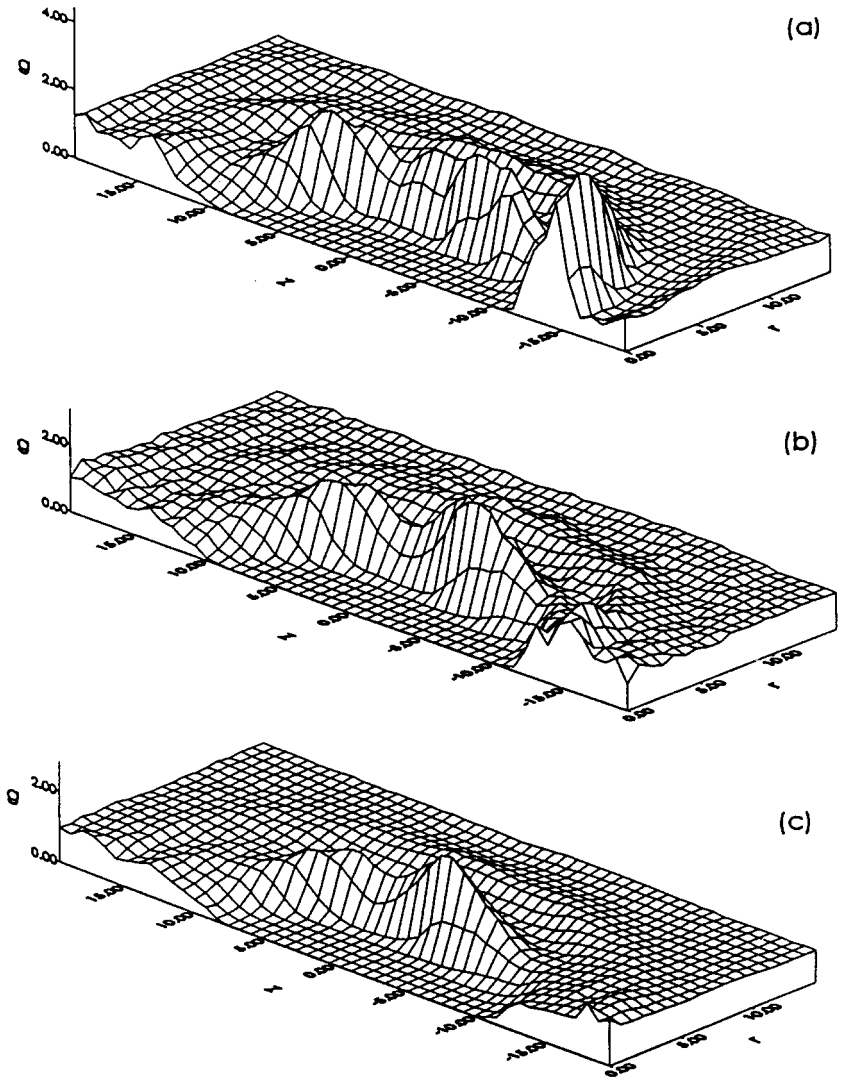


Figure 8. Centre of mass two-variable pair distribution functions for the 200 molecule system in the nematic state at 330 K. The distances are measured in Å. (*a*) System with charges (table 7, column 4) after 1000 ps of equilibration; (*b*) 20 ps after switching off the electrostatic interactions; (*c*) 100 ps after switching off the electrostatic interactions.



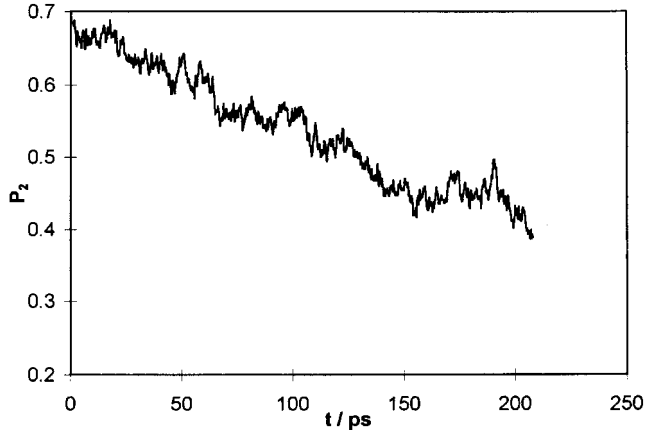


Figure 9. Order parameter ($P_2$) variation after switching off the electrostatic interactions in the nematic state at 330 K.

reinstall the local order which is determined by molecular properties, but not by the starting configuration.

It is clearly seen that the distribution functions in the nematic and isotropic phase are strikingly similar [compare figures 8(*a*) and 11]. In the isotropic phase, features are less pronounced: peaks at $(z, r) = (-0{\cdot}5, 0{\cdot}5)$ and $(0{\cdot}5, 0{\cdot}5)$ have heights about 2·5 in the nematic phase and about 2 in isotropic state. The peak at $(z, r) = (-1{\cdot}5, 0{\cdot}2)$ changed similarly and only that at $(-0{\cdot}7, 0{\cdot}5)$ is not seen as a shoulder of the peak at $(-0{\cdot}5, 0{\cdot}5)$. One can conclude that the *local* structure, which is determined by the short range molecular interactions, is similar in the nematic and the isotropic phase and only at long distances can the effect of the nematic ordering be seen.

More comprehensive information about the molecular symmetry effect on the distribution function can be gained if one separates it into parts originating from

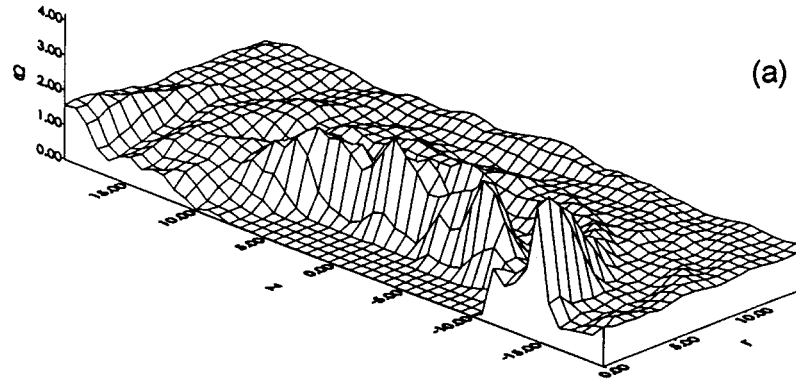


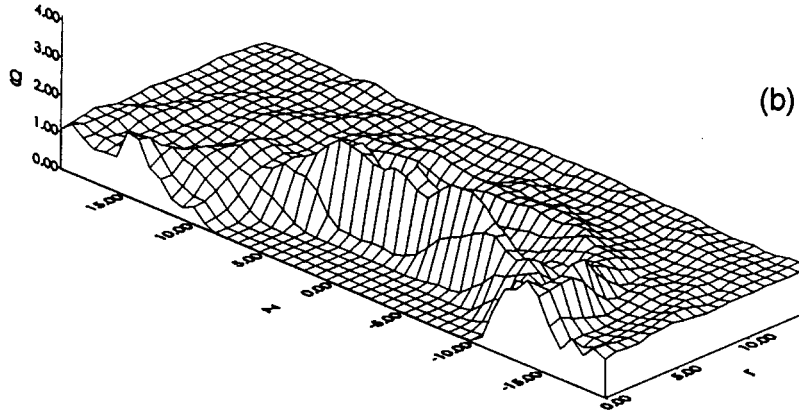


Figure 10. Centre of mass two-variable pair distribution functions for a 100 molecule system in the nematic state at 333 K from simulations of [8]. The charges are positioned only at the CN fragment. (*a*) $q = 0{\cdot}5$ e; (*b*) $q = 0{\cdot}28$ e. The distances are measured in Å.

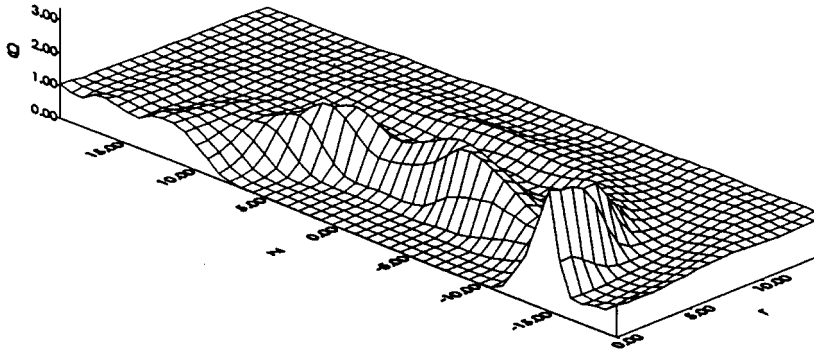

Figure 11. Centre of mass two-variable pair distribution functions for the 200 molecule system in the isotropic state at 330 K. The distances are measured in Å.

parallel and antiparallel oriented molecules (figure 12). To obtain the functions in figure 12 we did not make special assumptions concerning the degree of parallelism at which the molecules can be treated as parallel, but separated them depending on the sign of the $\cos \Theta$ between the pair of molecules under consideration, where $\Theta$ is the angle formed by two molecular $z$ axes. One can see that the peak at $z = -1{\cdot}5$ nm is present only in the antiparallel part. This can be explained by the presence of the strong dipole moment at the cyano groups and is confirmed by the disappearence of this peak on switching off the charges (see figure 8). Localization of a strong dipole moment within one fragment facilitates dimer formation. This effect is known for cyano derivatives (see, for example [31]), but MD simulations make it uniquely possible to look at the peculiarities of this phenomenon and its dependence on the molecular structure.

In table 7 partial charges for the three mesogens CB5, PCH5 and CCH5 are presented. For PCH5 and CB5 two kinds of charge distribution are presented. In the first column for each substance the Mulliken charges

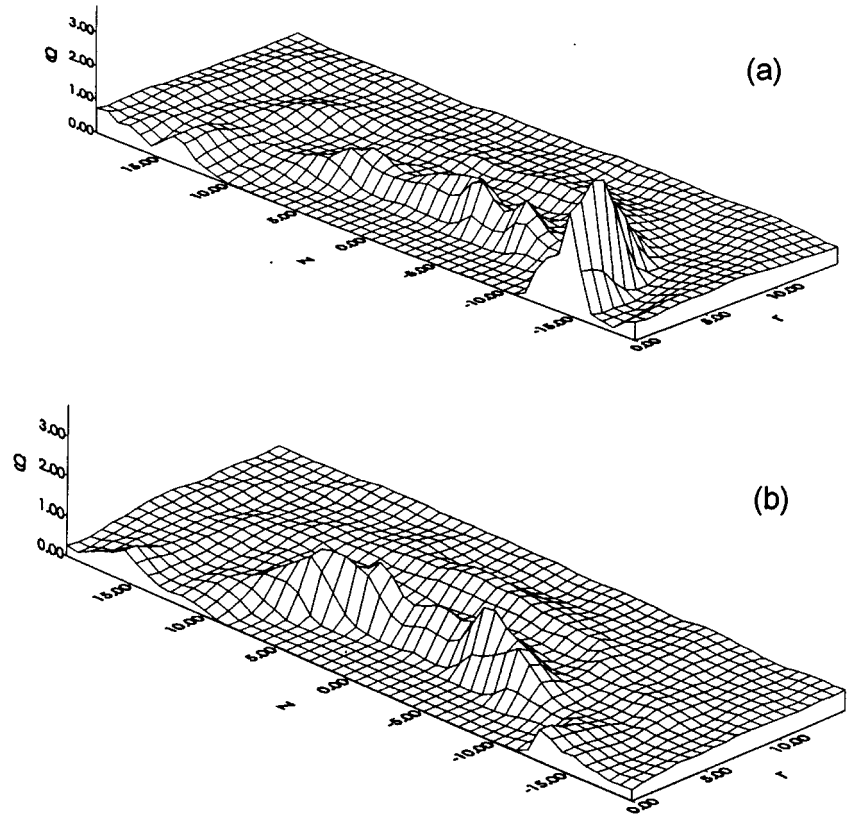


Figure 12. Centre of mass two-variable pair distribution functions for the 200 molecule system in the nematic state at 330 K. The distances are measured in Å. (*a*) For anti-parallel molecules; (*b*) for parallel molecules.



are given, and in the second column the charges used in simulations. It should be noted that Mulliken charges do not reproduce the electrostatic potential obtained from the *ab initio* calculations. Similarly, a simple summation of the charges from the FA approach for each UA results in an electrostatic potential which differs from the one calculated with the charges obtained with a UA model fitting. This is confirmed also by the difference in the dipole moments received for the different sets of charges (see table 7). Due to the long range character of electrostatic forces, this influences the whole structure of the simulated substance. Because of this we used a fitting procedure as described in §2 to receive the partial charges and used only these during the simulation. CB5 was simulated in [32] also within the united atom approach (slightly different interaction potential and a different number of atoms) taking into account also molecular flexibility and electrostatic interactions. Molecules of CB5 and PCH5 have very similar shapes (and consequently repulsive parts of the potential) and the same numbers of carbon atoms, but the partial charges used in the simulation and the dipole moments are strongly different. CB5 has a partial charge for nitrogen very close to that of PCH5. Due to conjugation, the rest of the molecular charge is more distributed along the molecule. This results in a bigger dipole moment. But despite the increase of the dipole moment, the peak height at $z = -1{\cdot}5$ nm is strongly decreased in CB5 [32]. This peak we identify with the presence of strongly coupled pairs. The decrease of the peak does not mean a decrease in the number of dimers, only that their geometry is changed. In PCH5 the dipole moment is more localized at the cyano group and its net charge in PCH5 ($-0{\cdot}07$) is smaller than in CB5 ($-0{\cdot}18$). This electrostatic repulsion of the cyano group leads to a stronger overlap of the molecules in CB5 dimers. CCH5 has much smaller partial charges, but also a very high net charge of the cyano group. Therefore one can conclude that while the overlapping of molecules of CCH5 as dimers will increase, the number of dimers may be the same as for CB5 or PCH5.

The number of molecules involved in dimers (or more strictly speaking in $N$-molecule aggregates) can be calculated directly from the simulation configurations. From the radial distribution function of the carbon atoms belonging to the cyano fragment [figure 13 (*a*)] one can conclude that the cyano groups of the molecules which form dimers in PCH5 are separated by not more than 0·43 nm. In general, any molecule can have more than one neighbour, whose cyano group gets into the first surrounding shell and thus bigger chains or aggregates of associated molecules can be formed. The fraction of

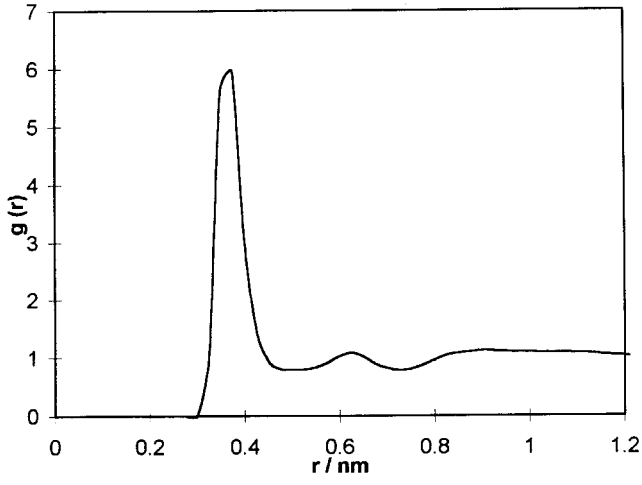


(*a*)

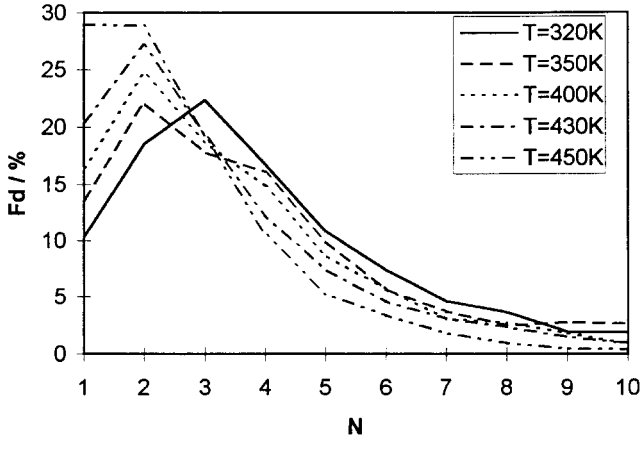


(*b*)

Figure 13. (*a*) Radial pair distribution function for the carbon atoms of the cyano fragment at 340 K; (*b*) The fraction of molecules in multimers containing $N$ molecules at different temperatures.

molecules involved in $N$-particle aggregates is shown in figure 13 (*b*) for several temperatures. The decrease of the average size of aggregate with temperature increase is clearly seen. The number of monomers is rather small: changing from about 10% at 320 K to about 30% at 450 K. But such a detailed distribution probably cannot be observed experimentally. From static properties, such as the static dielectric susceptibility, one cannot specify the existence of $N$-mers. Therefore, to compare our distribution with some experimental value we roughly estimated the Kirkwood factor $g_1$ basing it on the relation [33]

$$g_1 = \frac{\sum_k N_k \mu_k^2}{\mu_m^2 \sum_k N_k} \qquad (11)$$

where $N_k$ and $\mu_k$ are, respectively, the number and the average dipole moment of associates of kind $k$. Using a very simplified model, where the dipole moment of all aggregates containing an odd number of molecules equals that of monomer $\mu_m$, the dipole moment of even number aggregates being zero, we obtained $g_1$ about 0·35 in the mesophase and $g_1 = 0{\cdot}54$ in the isotropic phase. The latter value is between the experimental values for CCH5 and CB5 [31].

### 3.6. *Translational and rotational diffusion*

The relaxation of the local structure, discussed in § 2.1, is intimately related with the single particle dynamics. Both properties equilibrate much faster than the collective variables (see also ref. [13]) and can follow closely the temperature variation within our simulation series. From figure 14 it is seen that translational self diffusion coefficients, calculated from the mean-square displacements of molecular centres of mass, obey rather well an Arrhenius type relation with almost equal values of activation energy along and perpendicular to the director (about 23 kJ mol$^{-1}$, respectively). The diffusion coefficient values are somewhat smaller than in the isotropic phase (see § 2.1.1) and reflect the anisotropy of the mesophase: the ratio $D_\parallel / D_\perp$ in the director frame is about 1·4 and approximately similar for all configurations. It should be noted that this ratio is smaller than in previous simulations [8] because there, translational diffusion was considered in a molecular frame.

Orientational diffusion in the nematic phase can be characterized by autocorrelation functions of the general form [21]:

$$C^L_{mn}(t) = \frac{\langle D^L_{mn}(0)\, D^{L*}_{nn}(t)\rangle}{\langle |D^L_{mn}(0)|^2\rangle}. \qquad (12)$$

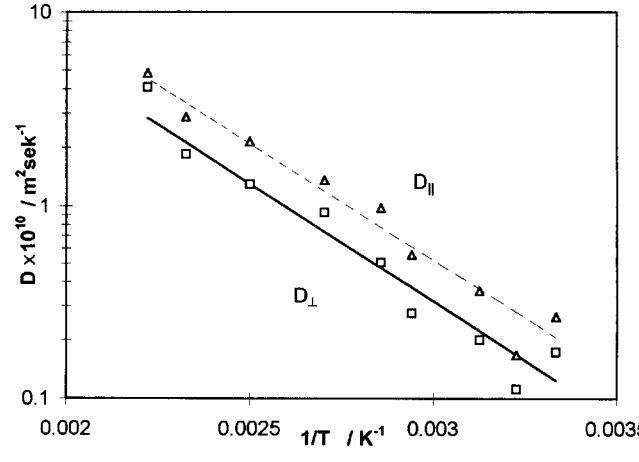


Figure 14. Temperature dependence of the diffusion coefficients $D_\perp$ and $D_\parallel$. The straight lines represent the least squares Arrhenius fit.

Taking into account the molecular dimensions of the mesogen, one can conclude that for sufficiently long time intervals reorientational motion is sufficiently well described by small-step rotational diffusion (this is confirmed by comparison of the orientational autocorrelation functions of different rank given in figure 3 for the isotropic phase). The rotational diffusion models for molecular motion in uniaxial mesophases are already well developed (see, for example [21]) and the following relations have been derived for the relaxation times of the autocorrelation functions of the first rank [34]

$$(\tau_{00}^{1\mathrm{rot}})^{-1} = D_{\perp}^{\mathrm{rot}} \frac{2-2P_2}{1+2P_2}$$
$$(\tau_{01}^{1\mathrm{rot}})^{-1} = D_{\parallel}^{\mathrm{rot}} + D_{\perp}^{\mathrm{rot}} \frac{1+2P_2}{1-P_2} \qquad (13)$$

where $D_{\perp}^{\mathrm{rot}}$ and $D_{\parallel}^{\mathrm{rot}}$ are the diffusion coefficients of tumbling and spinning motions, respectively. As is seen from figure 15, reorientational motion in our system is highly anisotropic and the relevant relaxation times are strongly temperature dependent. This coincides with the predictions of formulae (13). But it is impossible to determine the diffusion coefficients because of the presence of the order parameters in these formulae, which are not well determined for our system.

## 4. Conclusions

This investigation was aimed at a study of the temperature dependence of the properties of a realistic model of a mesogen. Therefore much attention was paid to adjusting molecular interaction parameters, responsible for electrostatic interactions, and equilibration of the whole system. It is clear that with contemporary computer power such simulations require rather prohibitive time. In many cases, especially when dealing with macroscopic parameters, the consequences of the system size and simulation time limitations are very well seen. Our simulations suggest that, in contrast to simplified models of mesogens, relaxation of macroscopic parameters till equilibrium is reached requires much longer times. Nevertheless, single particle dynamics, local processes such as dimerization, or conformational transformations can be successfully studied by computer simulations.

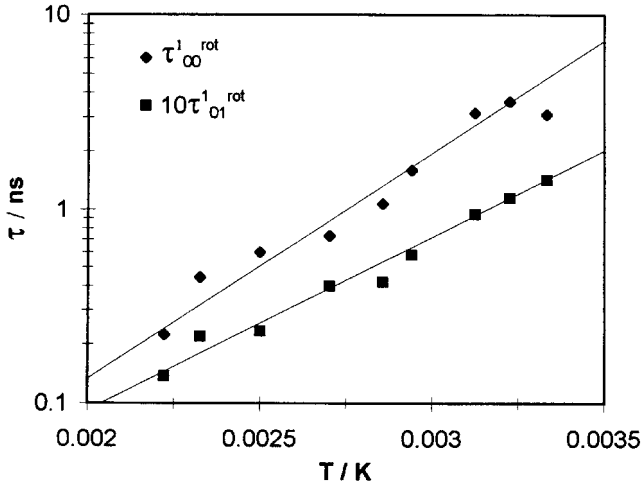


Figure 15. Temperature dependence of the relaxation times of the orientational autocorrelation functions of the first rank of different symmetry.

Financial support of the Deutsche Forschungsgemeinschaft and Fonds der Chemischen Industrie is gratefully acknowledged.

## Appendix

*Relation between the finite and infinite system order parameters*

The behaviour of the orientational modes in nematics has been treated in [24]. Such modes involve rotation of the director (unit vector **n**) around an axis in the $xy$ plane ($z$ being directed along the average director) through an angle which varies with position as $\cos(\mathbf{q}\ \mathbf{R})$. Following this treatment, we assume a small amplitude for each mode and identify the angle $\hat{\mathbf{n}}\mathbf{z}$ with the projection of **n** on the $xy$ plane. The random phase approximation is implied to be valid for our case, i.e. the effect of different modes on the director orientation in order to be statistically independent. It has been shown [24] that for each value of **q** there are two principle polarizations: one involving twist and bend, another—splay and bend distortions. Their mean square amplitude is given by

$$\langle n_{\alpha}^2(q)\rangle = \frac{k_{\mathrm{B}}T}{V(K_{33}q_z^2 + K_{\alpha\alpha}q_{\perp}^2)} \qquad \alpha = 1, 2 \qquad \text{(A1)}$$

where $k_{\mathrm{B}}$, $T$ and $V$ are the Boltzmann constant, the temperature and the volume of the sample, respectively; $K_{\alpha\alpha}$ are the three elastic constants. The excitation of such distortions causes the order parameters in the local and laboratory frames to differ. The effect of a single mode can be estimated by using the addition theorem for spherical harmonics, or Wigner $D$-functions, in a more general case [35]. Taking into account the axial symmetry of nematics, the statistical ordering within the box, as well as fluctuations of the box orientation, this yields

$$P_L^{\mathrm{lab}} = P_L^{\mathrm{loc}} P_L(n_z) \approx P_L^{\mathrm{loc}} \left[1 - \frac{1}{4}L(L+1)\langle n_{\alpha}^2(q)\rangle\right] \qquad \text{(A2)}$$

to the first order in $\langle n_{\alpha}^2(q)\rangle$. Hence the effect of all such modes in the random phase approximation can be

written [36]:

$$P_L^{\text{lab}} = P_L^{\text{loc}} \prod_{\alpha,q_i} \left[ 1 - \frac{1}{4} L(L+1) \langle n_\alpha^2(q) \rangle \right] \approx P_L^{\text{loc}} \exp\left[ -\frac{1}{4} L(L+1) \sum_{\alpha,q_i} \langle n_\alpha^2(q) \rangle \right]. \quad \text{(A3)}$$

For the summation over modes with different wave vectors $\mathbf{q}$ one can use the periodic boundary conditions implicit in the computer simulation procedure and the fact that this period is vanishingly small in comparison with the macroscopic dimensions of the real sample: the sum can be replaced by an integral with the number of independent modes $dN$ in the volume element in the $q$-space given by

$$dN\alpha = \frac{V}{(2\pi)^3} dq_x\, dq_y\, dq_z.$$

Consequently

$$\sum_{\alpha,q_i} \langle n_\alpha^2(q) \rangle = \sum_\alpha \frac{k_B T}{(2\pi)^3} \int_0^{q_x^m} \int_0^{q_y^m} \int_0^{q_z^m} \frac{dq_x\, dq_y\, dq_z}{K_{33} q_z^2 + K\alpha\alpha q_\perp^2} \quad \text{(A4)}$$

where $q_i^m = 2\pi/a_i$ is determined by box size. Accounting for the axial symmetry of nematics one finally obtains after integration and substitution into equation (A3):

$$P_L^{\text{lab}} = P_L^{\text{loc}} \exp\left\{ -\frac{1}{4} L(L+1) \sum_\alpha \frac{k_B T}{2\pi K\alpha\alpha a_z} \times \left[ \varepsilon \arctan\left(\frac{1}{\varepsilon}\right) + \frac{1}{2} \ln(\varepsilon^2 + 1) \right] \right\} \quad \text{(A5)}$$

$$\varepsilon = \frac{a_z}{a_\perp} \left( \frac{K\alpha\alpha}{K_3} \right)^{1/2}.$$

It should be mentioned that the effect of the director fluctuations on the nematic orientational distribution function has already been considered in [37]. But pursuing more general goals, the author of [37] did not derive an analytical solution of the problem even in the single-constant approximation. On the other hand, unlike in [37] and [29] in deriving equation (A5) we did not use a spherical cut-off approximation allowing the simulation box to be elongated in the nematic symmetry axis direction.



## References


[1] Tsykalo, A. L., and Bagmet, A. D., 1978, *Mol. Cryst. liq. Cryst.*, **46,** 111.

[2] Allen, M. P., 1990, *Phys. Rev. Lett.*, **65,** 2881.

[3] Paolini, G. V., Ciccotti, G., and Ferrario, M., 1993, *Mol. Phys.*, **80,** 297.

[4] Lee, S. H., Kim, H. S., and Pak, H., 1992, *J. chem. Phys.*, **97,** 6933.

[5] Luckhurst, G. R., Stephens, R. A., and Phippen, R. W., 1990, *Liq. Cryst.*, **8,** 451.

[6] Picken, S. J., van Gunsteren, W. F., van Duijnen, P. T., and de Jeu, W. H., 1989, *Liq. Cryst.*, **6,** 357.

[7] Wilson, M. R., and Allen, M. P., 1992, *Liq. Cryst.*, **12,** 157.

[8] Kroemer, G., Paschek, D., and Geiger, A., 1993, *Ber. Bunsenges. phys. Chem.*, **97,** 1188.

[9] Komolkin, A., Laaksonen, A., and Maliniak, A., 1994, *J. chem. Phys.*, **101,** 4103.

[10] Yoneya, M., and Berendsen, H. J. C., 1994, *J. phys. Soc. Jpn.*, **63,** 1025.

[11] Glaser, M. A., Malyzbender, R., Clark, N. A., and Walba, D. M., 1994, *J. Phys: Condens. Matter*, **6,** Suppl. 23A, A261.

[12] (*a*) Chalam, M. K., Gubbins, K. E., de Miguel, E., and Rull, L. F., 1991, *Mol. Sim.*, **7,** 357; (*b*) Emsley, J. W., Luckhurst, G. R., Palke, W. E., and Tildesley, D. J., 1992, *Liq. Cryst.*, **11,** 519

[13] Yakovenko, S., Muravski, A., Eikelschulte, F., and Geiger, A., 1996, *J. chem. Phys.*, **105,** 10 766.

[14] Gromos, 1987, *Groningen Molecular Simulation* is a software package developed by W. F. van Gunsteren and H. J. C. Berendsen, University of Groningen.

[15] Rykaert, J. P., Cicotti, G., and Berendsen, H. J. C., 1997, *J. comput. Phys.*, **23,** 327.

[16] Berendsen, H. J. C., and van Gunsteren, W. F., 1997, *Mol. Phys.*, **34,** 1311.

[17] Frisch, M. J., Trucks, G. W., Head-Gordon, M., Gill, P. N. W., Wang, M. W., Foresman, J. B., Johnson, B. G., Schlegel, H. B., Robb, M. A., Replogle, K. S., Gomperts, R., Andres, J. L., Roghavachari, K., Binkley, J. S., Gonzalez, C., Martin, R. L., Fox, D. J., Dofrees, D. J., Baker, J., Stewart, J. J. P., and Pople, J. A., 1992, *Gaussian 92* (Revision A), Gaussian Inc., Pittsburgh PA.

[18] Wilson, M. R., and Allen, M. P., 1991, *Mol. Cryst. liq. Cryst.*, **198,** 465.

[19] Holz, M., Private communication.

[20] Atkins, P. W., 1986, *Physical Chemistry*, 3rd Edn, (Oxford: Oxford University Press), p. 678.

[21] Zannoni, C., 1994, *The Molecular Dynamics of Liquid Crystals*, edited by G. R. Luckhurst and C. A. Veracini (Dordrecht: Kluwer Academic Publishers), Chap. 2, 6.

[22] Keyes, T., and Kivelson, D., 1972, *J. chem. Phys.*, **56,** 1057.

[23] Faber, T. E., 1989, *Proc. r. Soc. London*, **A375,** 579.

[24] De Gennes, P. G., 1974, *The Physics of Liquid Crystals* (Oxford: Clarendon Press), p. 333.

[25] Memmer, R., Kuball, H. G., and Schönhofer, A., 1993, *Liq. Cryst.*, **15,** 345.

[26] Hauptmann, S., Mosell, T., Reiling, S., and Brickmann, J., 1996, *Chem. Phys.*, **208,** 57.

[27] Faber, T. E., 1977, *Proc. r. Soc. London*, **A353,** 261.

[28] Faber, T. E., 1977, *Proc. r. Soc. London*, **A353,** 276.

[29] Bradshaw, M. J., McDonnell, D. G., and Raynes, E. P., 1981, *Mol. Cryst. liq. Cryst.*, **70,** 289.

[30] Seeliger, R., Haspeklo, H., and Noack, F., 1983, *Mol. Phys.*, **49,** 1039.

[31] Toriyama, K., and Dunmur, D. A., 1985, *Mol. Phys.*, **56,** 479.

[32] Komolkin, A., and Maliniak, A., 1995, *Mol. Phys.*, **84,** 1227.

[33] Cole, R. H., 1995, *J. Am. chem. Soc.*, **77,** 2012.
[34] (*a*) Fontana, M. P., 1994, *The Molecular Dynamics of Liquid Crystals*, edited by G. R. Luckhurst and C. A. Veracini (Dordrecht: Kluwer Academic Publishers), Chap. 16. (*b*) Ferrarini, A., Nordio, P. L., and Moro, G. J., 1994, *The Molecular Dynamics of Liquid Crystals*, edited by G. R. Luckhurst and C. A. Veracini (Dordrecht: Kluwer Academic Publishers), Chap. 3.
[35] Varshalovich, D. A., Moskalev, A. N., and Khersonskii, V. K., 1988, *Quantum Theory of Angular Momentum* (World Scientific), Chap. 1–4.
[36] Faber, T. E., 1977, *Proc. r. Soc. London*, **A353,** 247.
[37] Sheng, P., 1976, *Solid State Commun.*, **18,** 1165.